Current trend in offshore wind energy sector and material requirements for fatigue resistance improvement in large wind turbine support structures – a review

Victor Igwemezie*†, Ali Mehmanparast*, Athanasios Kolios*

*Offshore Energy Engineering Centre, Cranfield University, Cranfield, Bedfordshire, England
†Materials & Metallurgical Engineering Department, Federal University of Technology, Owerri
*†corresponding author email address: victor.Igwemezie@cranfield.ac.uk

Abstract

At present, the UK government is driving the survival of the wind energy industry by using interventions that encourage investment in the sector. The use of a Contract for Difference (CfD)/Strike price model by the UK government supports the wind industry and guarantees that wind energy generators have a stable premium over a period of 15 to 20 years; however, this may not last forever. The growth and stability of the wind industry will depend essentially on continued reductions in wind energy cost, even below that of fossil-fuel based energy sources. Huge cost reduction beyond the present strike price of £57.50/MWh for some projects to be delivered in 2022/2023 may be achieved quickly through efficient and optimized turbine support structure. Consequently, the offshore wind industry is currently making enormous efforts to upscale wind turbines (WTs) from 8MW to 9.5MW,10MW and then 12MW HAWT (Horizontal Axis Wind Turbine). This level of upscaling no doubt creates tough challenges because the mass of the turbine increases linearly with the cube of the rotor radius. Monopiles having diameters larger than 7m have been proposed, with a wall thickness section in the range of 70 to 110mm. It is generally thought that Thermo-Mechanical Controlled Process (TMCP) steels are well suited for extra-large (XL-WTs). This paper reviews the present status of WTs and critically assesses the material factors in the structural integrity concerns that may confront the use of XL steel plates in the design of XL-WT support structures.

Key words: XL wind turbines, offshore wind, monopile, TMCP steels, structural integrity

Contents

Nomenclature

a_o	Initial crack length		LCOE	Levelized Cost of Energy
a_f	Final crack length		FID	Final Investment Decision
σ_y	Yield stress		HAWT	Horizontal axis wind turbine
σ_{UTS}	Ultimate tensile stress		LEFM	Linear Elastic Fracture Mechanics
$\Delta\sigma$	Cyclic stress range		OWT	Offshore WT
ΔK	Cyclic SIFR		SLIC	Structural Lifecycle Industry
da/dN	Fatigue crack growth rate (m/cycle)			Collaboration Joint Industry Project
P_{max}	Maximum load		SW	Seawater
P_{min}	Minimum load		TMCP	Thermo-mechanical controlled
K	Stress intensity factor (SIF)			process
R	Stress ratio		WT	Wind turbine
CFCG	Corrosion-fatigue crack growth rate		XL	Extra-Large
R			HAZ	Heat affected zone
FCG	Fatigue crack growth		DBTT	Ductile to brittle transition
FCGR	Fatigue crack growth rate			temperature
SIFR	Stress intensity factor range		CCT	Continuous cooling temperature

1. Introduction

This paper reviews the present status of wind turbines (WTs) and the economic perception of extra-large wind turbines (XL-WTs). It also presents some critical structural integrity concerns relating to XL steel plates, which need to be evaluated to enable technical and cost-effective decisions to be made for the design of next generation WT support structures.

Wind power is recognized as having enormous potential in meeting the European Union 2020 and 2030 renewable energy targets [1][2] and the long term reduction of greenhouse gas emissions by at least 80% by the year 2050 as compared with 1990 levels [3][4]. Wind energy accounted for about 49.2% of all the renewables generated in UK for the second quarter of 2018 [5]. A modern single 1.5MW WT can generate sufficient energy to meet the annual needs of 332 homes, and a 2.5MW WT can generate enough electricity to power over 1,400 homes for a year, enough to power an average computer for more than 2,000 years, or sufficient to make 230 million cups of tea [6]. A 1GW wind farm can power just over one million homes while a 10GW wind farm serves the energy needs of over 7.5 million UK households a year [6][7]. Due to the capacity of this form of renewable energy source, it has witnessed increased use to power, from small and medium sized businesses, and local communities to large commercial environments in countries with enough wind resources.

A typical WT is reported to generate about 70 – 85% electricity at a time, depending on the speed of the prevailing wind. The wind speed is a limiting factor to the amount of energy that can be produced. Nevertheless, the sector is now well established as a major part of the UK's low carbon energy mix.
Fig. 1(a) shows a live chart of energy mix as extracted from MyGridGB [8] on 03 September 2018.
Fig. 1(b) shows electricity supplied by the Renewable Energy Company Ltd, trading as Ecotricity. About 98TWh of renewable electricity was generated in 2017 which is an increase of 18.8% against 2016 records [9]. This increase has been attributed to bigger wind turbines and higher wind speeds. Onshore wind is said to generate over 50% of renewable power and there are large numbers of projects under development for offshore wind power [2][10]. The UK government is very much committed to the development of this sector by increasing subsidies and planning for a biannual contract for difference (CfD) auction to increase offshore wind capacity [2].
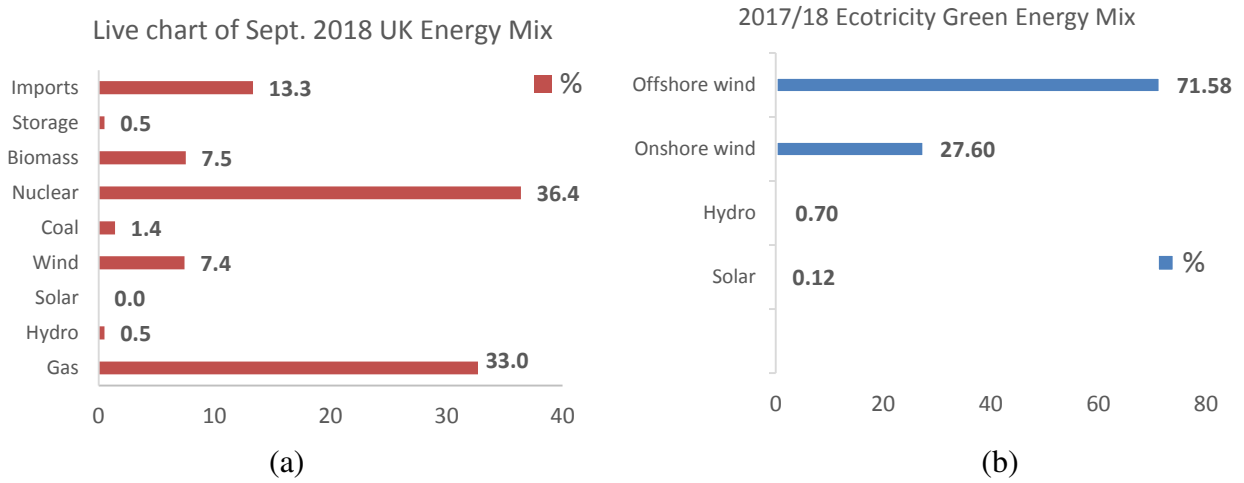
Fig. 1: (a) Plot of Live Chart of energy supply mix in the UK, Sept. 2018 (MyGridGB) [8] (b) 2017/2018 Ecotricity green energy supply mix (Adapted from [11])

As at the end of 2017, UK has the world's largest offshore wind market and with the highest installed global capacity of about 35.7% (5.8GW) for operating offshore wind capacity [12][13]. If China is excluded, UK then has the largest global capacity of offshore wind projects under construction (2.6 GW) [12].The UK appears to have succeeded because its government is driving the survival of the OWT industry by using an intervention scheme [14], thereby making it somewhat competitive with non-renewable based energy sources. In fact, towards the end of 2017, BEIS published the outcome of the second Contracts for Difference (CFD) allocation round and three offshore wind developers won a strike price as low as £57.50/MWh for projects to be delivered between 2022 and 2023 in England and Scotland [15].

From the foregoing, continued investment in wind energy will be determined largely by the ability of the industry to continue to achieve reductions in wind energy cost . A study on the Long-term Trends in Wind Energy LCOE [16] shows a steady decline in the cost of energy over time – in fact up to 35%-40% reduction in LCOE by 2030. This hypothetical exercise can only be achieved by considering some factors listed in the report, which include performance improvements of the turbines and support structure/tower concepts. A large wind energy cost contribution comes from the turbines [17]. Although it is ahead of the set milestones, substantial cost reduction can be made in this area by efficient and optimized turbine design.

2.   The current status of wind turbines

The largest WTs currently installed and functional with power ratings of 8MW are the Siemens Gamesa SG 8.0-167 DD,   MHI Vestas V164-8.0MW and Areva 3-bladed 8MW [18][19][20]. This 8 MW WT has been used in the Burbo Bank Extension wind farm [21][22] (see also [19][23]). To stay ahead and to achieve high design efficiency, the industry is currently making intense efforts to upscale WTs from 8MW to 9.5MW,10MW and then 12MW HAWT. The strike price of £57.50/MWh won by Moray Offshore Windfarm (East) Limited in 2017 is partly due to anticipated use of MHI Vestas V164-9.5MW WT for the 950MW capacity Moray East wind farm, expected to be commissioned around 2022 and 2023. Currently, General Electric is investing in the development of 12MW Haliade-X – which will be recorded as the world's biggest OWT, to be available in 2021 [24][25]. This level of upscaling no doubt creates tough challenges because the mass of the turbine increases linearly with the cube of the rotor radius [26]. This trend can be seen in Fig. 2, which shows the increase in the size of the support structure with rotor diameter. The update is informed by
Table 1 which is mainly theoretical concepts found in the literatures and works of [27][28][29][30][31][32].
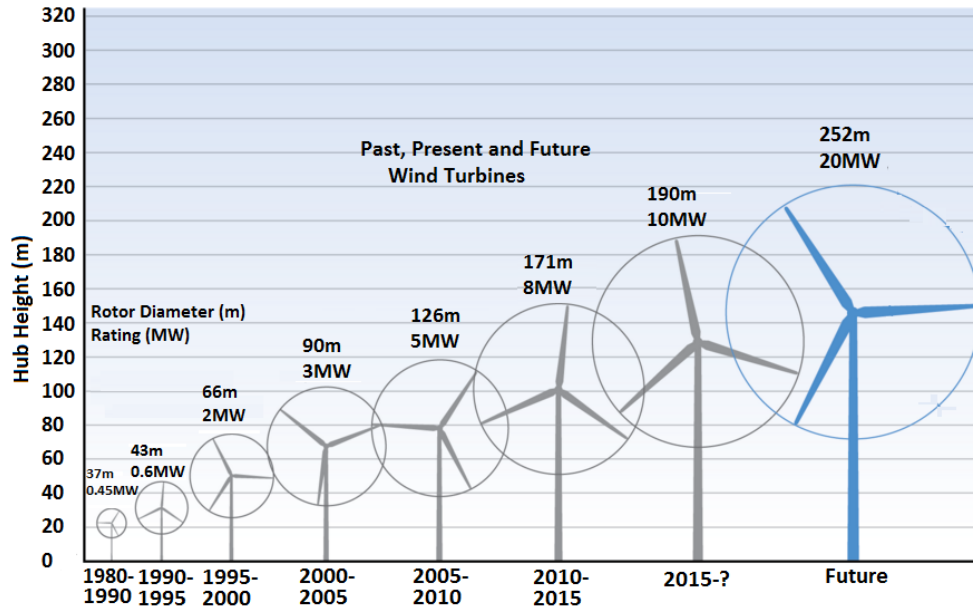
Fig. 2: Growth in size (and power) of horizontal axis wind turbine (HAWT) (Adapted from [33][34]).

Table 1: 3 Bladed 10MW HAWT under development

3 Bladed 10MW HAWT	Rated Wind speed (m/s)	Rotor diameter (m)	Ref.
DTU 10MW Reference Wind Turbine	11.4	178.3	[35]
AMSC SeaTitan 10MW Wind Turbine Model	11.5	190	[28]
10MW Wind Turbine Model	12	170	[29]
Rotor Design 10MW Offshore Wind Turbine Model	13.25	141	[30]
*SWAY 10MW-1-bladed Wind Turbine Model	13.4 (Approx.)	164	[31]

From the foregoing, high level industry achievement has been made so far and the offshore wind sector has delivered 20.9TWh of electricity onto the national grid in 2017, while that of onshore wind delivered 29.1TWh [36]. This capacity can generate enough electricity to meet the needs of over 3.2 million UK households. In 2017, the wind energy sector is reported to have supplied the electricity needs of 5.3 million homes in the UK. Analysis has shown that deep offshore designs will contribute immensely in lowering the LCOE in offshore wind energy by unlocking the offshore market potential in the Atlantic, Mediterranean and deep North Sea waters [37]. It is reported [37] that deep waters in the North Sea alone could provide turbine energy capable of meeting the EU's electricity consumption four times over. To harness better energy resources at sea, the offshore energy industry is frantically researching and developing concepts for offshore wind farms in deeper waters. Fig. 3 shows global offshore wind projects at various water depths and distances from the shore with the project phase colour-coded [38]. The figures show that some projects are being planned for water depths up to 50m.

3. Support structure for large wind turbines

As aforementioned, wind energy providers are assiduously pushing towards reduction of the cost of energy. Experience with the technology has revealed that environmentally friendly and economical wind energy can be produced by increasing the size of the turbine [23]. This simply means that as the turbines become bigger more green energy is generated and our environment is the better for it [39].
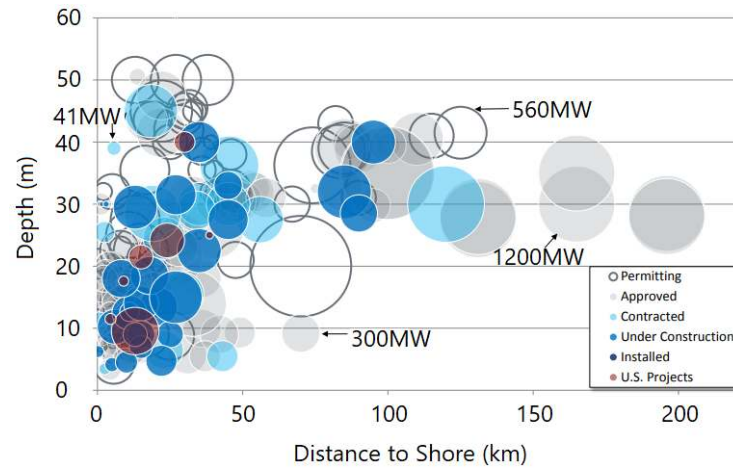
Fig. 3: Average water depth vs. distance to shore for global offshore wind projects where the bubble size represents project rated capacity (in MW) [38]. (Reproduced with permission)

The monopile is the commonly used support structure for WTs. This is due to their ease of design and manufacture, as compared with other foundation concepts. Also, monopile is very suitable for water depths up to 30m and well-suited to mass production, has a conventional impact driving installation method and remains rigidly in position in most soil conditions [40]. At up to 30m depth, the monopile has clearly more commercial and technical advantages.

As offshore activity is now moving into deeper waters, there is ongoing research on which support structure is suitable. There are four common types of OWT foundations – gravity based, monopile, tripod and jacket – other modifications are simply based on these four, as shown in Fig. 4.
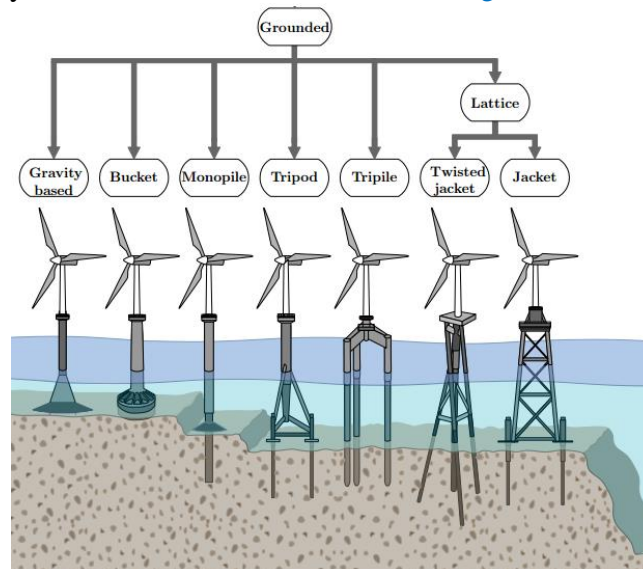

Fig. 4: Most common grounded turbine support structures and some of their modifications [32] See also [37][41]. [This figure is used under MDPI Open Access Information and Policy]

Beyond 30m water depth, other types of foundation structure start gaining preference over the monopiles. One report states that about 96% of the presently commissioned OWTs are supported on monopile structures while the remaining 4% are supported on jacket structures [31]. Some of the existing and conceptualized solutions for water depth above 30m are shown in Fig. 5. These floating WTs are increasingly gaining acceptance and deployment. They offer great means of expanding the wind energy potential and reducing energy cost. Since the successful commissioning of the first floating wind turbine - Hywind Scotland, in 2017 the technology has seen an increasing interest by investors. Other pioneering floating WTs in operation are the Fukushima Phase 1&2 5MW that started operation in 2017[42]; Fukuoka with total 7.5MW that

started operation in 2018 [42]; The WindFloat Atlantic project, Viana do Castelo Portugal [43]; Dounreay Trì Scotland, started in 2017 and expected to be commissioned in 2020; Floatgen, France's first offshore floating WT commissioned in 2017 [44]; and Kincardine Floating Offshore Wind Farm projects are expected to be completed in 2020 [45]. The 24MW Groix offshore wind and 24.6MW Elomed Gruissan in France are expected to go commercial in 2020 and 2021 respectively. The Provence Grand Large in Faraman, France is to be deployed in 2020 and will use 8MW Siemens WTs [38]. This indicates an increase in the size of the support structure for modern floating WTs.
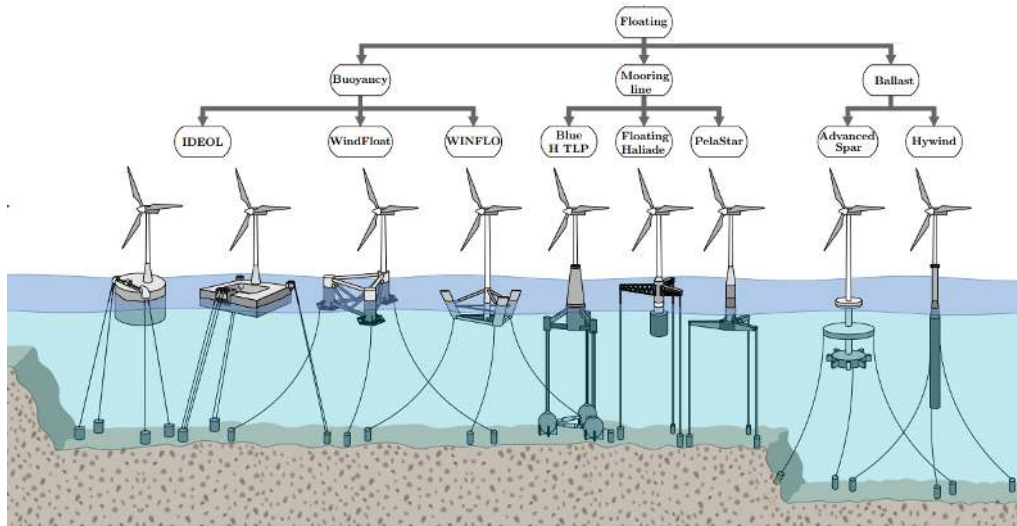

Fig. 5: Existing floating solutions and proposed deep water support structures for WTs [32] see also [37][46]. [This figure is used under MDPI Open Access Information and Policy]

Bak et al. [23] presented studies on the dynamic loading and long-term cyclic WT loading on these alternative foundations. Consequently, jacket structures tend to be favoured beyond 30m water depths, up to 50m. These types of studies are giving impetus to the shift of attention to alternatives such as multi-pod foundations (e.g. jacket, tetrapod and tripods) supported on shallow foundations to reduce the environmental effects of piling noise [47]. They are reported to offer about 50% reduction in the quantity of steel used for their manufacture compared with the monopile structure [48]. This may form one of the reasons for their serious consideration and related foundation type for larger turbines in deeper waters [49]. However, the choice of substructure type largely depends on the nature of loads to be supported, water depth, soil conditions, storage requirements, manufacturing, installation, and transportation cost.

4.   Offshore wind turbines and size of monopile

Many of the newly licensed wind farms in Europe, especially in UK Round 3 and Germany, to be developed before 2020 are at a water depth of 40m or more. Despite the studies, it appears that monopile structures are still gaining more attention from developers and from 10MW concept designs (see
Table 1 references). Following the results of advanced finite element (FE) modelling, highly optimized design methods and experiences from full-scale measurements, suggestions have been made regarding the possibility of using monopiles for water depth above 30m [50].

The Gemini Wind Farm of 150 WTs of the Siemens SWT-4.0-130 model with a production capacity of 4MW each and a total capacity of 600MW, sited 85km from the coast of Groningen in the Dutch part of the North Sea in water depths up to 37m, is reported to be one of the world's largest wind farms currently in existence [51]. The wind farm is fully commissioned and is expected to serve the energy needs of about 785,000 households or 1.5 million people, reducing CO_2 emissions by 1.25 million tons per annum [51][52][53]. The yearly power production is expected to reach 2.6TWh and ultimately will add towards reducing the cost of wind energy in the Netherlands and Europe. The WT in this project is supported by a monopile with a base diameter of 7m and top diameter of 5.5m, with each steel monopile weighing 670 – 916 tons [53][54].

Veja Mate Wind Farm has 67 turbines of the Siemens SWT-6.0-154 model with 6MW each and a total capacity of 402MW, sited in the North Sea at a distance of 95km from the shore. It is capable of powering about 285,000 homes with a reduction in CO_2 emissions of about 575,000 tons per annum and SO_4 of about 13,400 tons per year [55]. The monopile diameter for this 6MW turbine capacity is expected to be from about 7.8m [53] and each steel monopile weighs about 1,300 tons. Also, the Gode Wind Offshore Wind Farm in the German North Sea is expected to use 97 Siemens 6MW WTs with a 7.5m diameter monopile [56].

The Burbo Bank Extension Offshore Wind Farm has 32 MHI Vestas V164-8.0MW turbines with a production capacity of 8MW each and a total capacity of 254.2MW. It is sited in the Irish Sea in a water depth a little above 30m and 11.5km distance from the shore. It is reported to have the capability of powering 180,000 homes with a reduction in CO_2 emissions of about 364,000 tons per annum and SO_4 of about 8,000 tons per year [57]. The monopile diameter for this 8MW turbine capacity is about 8 to 9m [35][58]. The V164-8.0MW turbine with same monopile diameter is expected to be used for the Moray Firth Eastern Development Area 2, with 93 turbines, and many others under construction across the UK, the Netherlands, Germany, etc.

Monopiles having a diameter larger than 7m are today referred to as extra-large (XL). Their general thickness is usually in the range of 70 to 110mm [53]. XL monopiles, with diameters up to 10m, are claimed to be feasible in water depths up to 60m [50][59]. There are current considerations to venture into production of monopiles with 10m diameter and 95mm thick [59]. However, the economic and technical feasibilities of XL monopiles in deeper water will pose enormous challenges as wave action will increasingly interfere with the dynamics of the turbine structure. XL monopiles can also be commercially unviable due to storage, transportation and installation logistics, although there are fewer transportation and installation constraints for offshore projects than onshore projects [38]. The challenges that the large thickness of these XL monopiles support structures can introduce in the structural integrity assessment are the major motivation for this paper and will be discussed shortly.

Economic efficiency is one of the most important considerations in the design of a WT support structure. Hence, there is a need to have a balance in the system components. Fig. 6 shows a typical costs breakdown for an OWT [60].
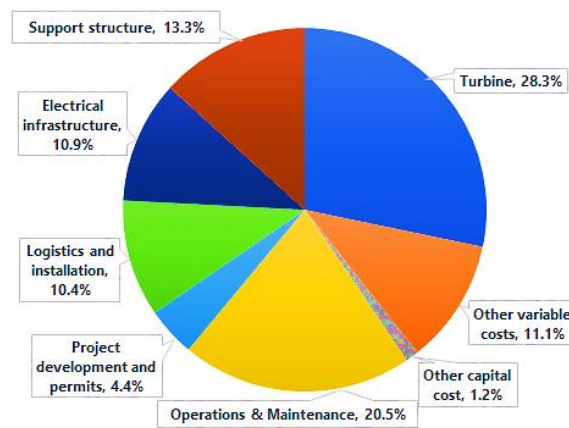
Fig. 6: (a) Estimated life- cycle cost breakdown for a typical offshore wind project, adapted from [60]. See also [61]

The support structure is typically made of 'high' strength steel and the price contribution is as high as 13.3%. The cost of transportation and erection of the components is a function of the materials used and subsequently the weight of the system. Since the height of a tower directly determines the energy yield, it is therefore quite important for the final cost of energy to build towers to be optimized and hence should be determined before the design process commences [62]. The steel structure of a WT is one of the most critical

parts in the wind energy development system [63]. This is because mistakes in steel selection and fabrication considerations will impact the cost and lead to the destruction of expensive blades and the nacelle/rotor system. Given the huge contribution of steel material cost in the overall cost of a WT, a material efficient design with satisfactory performance becomes an important step in the manufacture of support structures.

5. Steel selection for offshore application

Some of the many grades of structural steel in Europe are: S195, S235, S275, S355, S420 and S460. Grades S235, S275 and S355 are the common structural steel grades in use across the EU for many construction projects [64]. Table 2 shows the typical steel grades and properties in use across the UK.

In 'European Standard classifications', structural steels are sub-graded and referenced using standard symbols such as, but not limited to: *S, JR, J0, J2, K2, W, Z, C,* etc., where S denotes structural steel. The sub-grades *JR, J0, J2, K2* refer to material toughness at a particular temperature, *W* denotes weathering steel, *Z* structural steel with improved strength perpendicular to the surface and *C* structural steel formed by cold working. The numerical digits following the symbol *S* shows the minimum yield strength of the steel. For instance, typical sub-grades of S355 steel are S355K2, S355J2 and S355JR. S355K2 is a structural steel with an impact resistant testing strength of 40J at a testing temperature of -20°C (K2); if given as S355K2W, the W means that this sub-grade has been designed with a chemical composition to resist increased atmospheric corrosion (weathering) (W) [64].

Table 2: EN10025: Parts 2 and 4 UK steel grades [65]

EN10025:Part2				
Grade	Yield (R_{eH}[a]) min Strength at t=16mm (N/mm²)	Tensile R_m[a]	Charpy v-notch longitudinal Temp(°C)	Energy (J)
S275JR	275	410/560	20	27
S275J0	275	410/560	0	27
S275J2	275	410/560	-20	27
S355JR	355	470/630	20	27
S355J0	355	470/630	0	27
S355J2	355	470/630	-20	27
S355K2	355	470/630	-20	40

EN10025: Part4				
Grade	Yield (R_{eH}[a]) min Strength at t=16mm (N/mm²)	Tensile R_m[a]	Charpy v-notch longitudinal Temp(°C)	Energy (J)
S355M	355	470/630	-20	40
S355ML	355	470/630	-50	27
S420M	420	520/680	-20	40
S420ML	420	520/680	-50	27
S460M	460	540/720	-20	40
S460ML	460	540/720	-50	27

Further letters and classifications based on chemical composition, manufacturing process and relevant application may be used to reference particular grades/products of structural steel. For example, S355J2+N is a structural steel with an impact resistant testing strength of 20J at a testing temperature of -20°C (J2) and has been given a normalized heat treatment (+N). 355JR steel is a high tensile strength structural steel which can be readily welded to other weldable steel. J denotes the notch impact test (done at; JR: room temp, J0: 0°C; J2: -20°C). The simple meaning is that S355JR can withstand an impact energy of 27J at 20°C, S355J0 can withstand an impact energy of 27J at 0°C, and S355J2 can withstand an impact energy of 27J at -20°C. The sub-grades are sometimes followed by a letter H, e.g. S355J2H, where H stands for hollow section. The *M-series* are TMCP steel equivalents where *M* denotes Thermo-mechanical controlled rolled.

The minimum yield for S355 steel is 355N/mm² (MPa) hence the name S355. The general chemical composition and mechanical properties of S355 are as shown in Table 3. Table 4 shows that S355 steel is generally a low carbon steel whose specifications offer 'high' yield strength and the value varies with the steel grade. Limited grades also contain the compositions that are in bold. The impact strength at different temperatures is seen to decrease due to the fact that steel tends to become brittle when the temperature drops. If a structure is likely to experience temperatures down to -20°C, it is better and safer to then choose S355J2 rather than S355JR or S355J0.

The minimum yield strength 355MPa is up to 16mm thickness. This means that this test was carried out on a specimen whose thickness is 16mm. The value of the yield strength decreases with an increase in plate thickness. It is pertinent for designers to note this. The tensile strength is generally between 470 – 630MPa for thickness up to 100mm.

Traditionally, European Standard EN10025 S355 (or EN 10225 S355) is the main structural steel typically in use for WT support structures [66][67] and different sub-grades of S355 are selected for use in offshore applications. The so-called modern material choices for offshore applications are S335G8+M, S355G10+M, S420G2+M, and S460G2+M steel sub-grades.

Table 3: (a) General composition of S355 (b) Mechanical Properties of EN 10025 S355. [68][69][70][71][72].

(a)

Composition $wt\%$ (max)	EN 10025 S355 [ASTM 572]						
Fe	C	Mn	Si	Cu	N	P	S
~ 97	~0.22	1.60	0.55	0.55	0.02	0.06	0.035
Cr	Ni	Mo	V	Al			
0.03	0.50	0.10	0.12	0.02 (min)			

(b)

Steel Designation (Density 7.85 g/cm³ {7850 kg/m³})							
Mechanical properties (strength at 16mm)	EN 10025 S355 − [ASTM 572] [BS 4360]						
	S355JR [A572]	S355J0 -	S355J2 -	S355K2 A656	S355M	S420M	S460M
σ_y (MPa)	355	355	355	355	355	420	460
σ_{UTS} (MPa)	470 -630	470 -630	470 -630	470 -630	470 -630	520-680	540 - 720
EL %	20	22	23	22			17
E (GPa)	210	210	210	210	210	210	210
v	0.3	0.3	0.3	0.3	0.3	0.3	0.3
Notch toughness longitudinal Energy (J)	27 @ 20 °C	27 @ 0 °C	27 @ -20 °C	40 @ -20 °C	40 @ -20 °C 27 @ -30 °C	40 @ -20 °C	40 @ -20 °C

Table 4 shows how the mechanical properties of S355 steel changes with an increase in material thickness for a normalized condition from an austenitization temperature of 870°C.

Table 4: Variation of mechanical properties of S355 steel with thickness [68][73]

Steel Designation (Density 7.85 g/cm³ {7850 kg/m³})			
Mechanical properties	EN 10025 S355 − [ASTM 572]		
	Normalized 870°C, air cooled		
t = thickness	t = 3-16	t = 16 - 40	t = 40 - 63
σ_y (MPa)	355	345	335
σ_{UTS} (MPa)	470 -630	470 -630	470 -630

These steel grades have been manufactured specifically for offshore pipelines, platforms, pressure vessels, and modern WT installations [74]. The G grades are hot rolled to give a fine-grained microstructure, vacuum degassed, fully killed. A typical chemical composition of this class of steel S355G10+M (manufactured by Dillinger Hütte) and the mechanical properties of different offshore grades are shown in Table 5.

Table 5: The chemical composition and mechanical properties of offshore steel grades [75]

Composition wt% S355G10+M								
Fe	C	Mn	Ni	Si	Cu	Cr	NB	P
~97.5	~0.06	1.57	0.33	0.27	0.24	0.034	0.022	0.013

Mo	N	Ti	V	S
0.006	0.004	0.003	0.001	0.0009

Steel Designation (Density 7.85 g/cm³ {7850 kg/m³})

Mechanical properties Hot rolled plate	EN10225 S355G10+M			
	S355G8+M	S355G10+M	S420G2+M	S460G2+M
σ_y (MPa)				
<Ø16mm	355	355	420	460
Ø16 - Ø25 mm	355	355	400	440
Ø25 - Ø40 mm	345	345	390	420
Ø40 - Ø63 mm	335	335	380	415
Ø63 - Ø100 mm	325	325	380	406 (63 -80) /400 (80 -100)
σ_{UTS} (MPa)				
<Ø40mm	470 - 630	470 - 630	500 - 660	~520 - 700
Ø40 < 100 mm	470 - 630	470 - 630	480 - 640	~500 – 675
BH	285	285	-	-
EL % (min)	22	22	19	17
E (GPa)	205	205	-	-
v	0.29	0.29	-	-
M %	55	55	-	-
Charpy V-notch (J)	50 @ - 40 ºC	50 @ - 40 ºC	50 @ - 40 ºC	-

$\emptyset \, (mm) = specimen \ thickness; \ \sigma_y = Tensile \ Yield \ strength;$
$\sigma_{UTS} = Ultimate \ Tensile \ Strength; \ BH = Brinell \ Hardness;$
$EL = Elongation \ at \ break; \ E = Modulus \ of \ Elasticity;$
$v = Poisson's \ Ratio ; M = Machinability$

In general, the grading system follows the kind of heat treatment and/or thermo-mechanical processing given to steel. So, we have normalized, normalized-rolled weldable fine grain structural steel while others are thermo-mechanically rolled weldable fine grain structural steels. It is extremely important that these steels are correctly specified, covering the strength grade and the steel sub-grade, in order to avoid brittle failure [65]. In other words, the intention of the structural classification is to serve as a guide in selecting the appropriate steel and a suitable inspection to avoid brittle fracture.

Selection criteria for steel material for marine structures are commonly based on properties such as strength, toughness and weldability. There are challenges in the optimum combination of high steel strength and large diameter tower in an attempt to reduce total steel tonnage per tower. The tensile ductility requirement considers the gap between yield strength and ultimate tensile strength. The wall thickness (δ) is an important criterion for tower stability and must be sufficient to withstand buckling of the tower wall. The optimum combination of tower wall thickness and shell diameter is a cost target.

The welding requirement considers the production of a good weld, which is critical, because there are long-term problems with *fatigue* and *cracks* in welded structures, and an increase in the thickness of steel plate increases this problem. The huge tower is also constrained by the physical capacity of specialist plate manufacturers and challenges associated with the welding of very thick steel plate [63].

6. Environmental loading on wind turbine support structure

WT support structures are exposed to high cyclic loading caused by wind and normal operation. If the structure is in an offshore environment, forces due to waves and sea current (tides) will be present.

Furthermore, forces due to mass, installation and maintenance activities also act on the structure. Gravitational and inertia forces are due to blade, tower and nacelle masses. The rotor blades experience bending moments in the edgewise direction caused by gravitational loads. For a pitch-controlled turbine, the bending may be in the flapwise direction. The bending moments vary cyclically due to operational rotation of the blades and the magnitude increases with the rotor diameter [76]. Other load conditions that may be considered are those due to operational centrifugal forces, Coriolis forces and gyroscopic forces. Centrifugal force acts outwardly due to rotation of the blade. Forces acting on a typical WT support structure are axial loads, lateral loads and bending moments, as shown in Fig. 7.
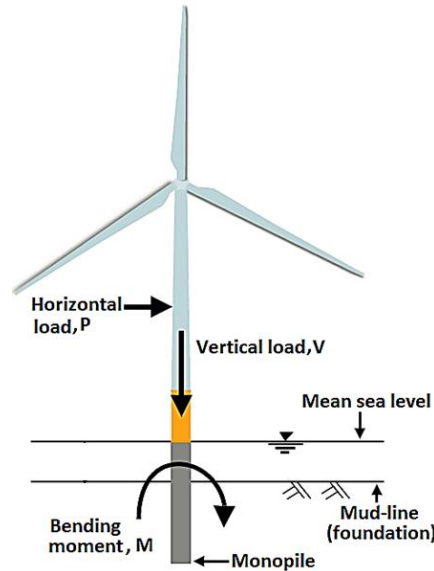

Fig. 7: Nature of loads on a monopile supported WT [47][77].

Torsional loading is sometimes considered. In other words, axial, lateral, bending and torsional vibrations are all present [49]. The predominant external loading problems come from wind and wave, particularly from wind loads [76].

OWT support structures also have to withstand some extreme loading events during their design life. External loading has two categories, the loading due to normal operating conditions and the extreme loading event occurring in a particular time, say once in 50 years of a wave height say 30m (i.e. 15m wave amplitude) or wind gust. These two conditions are usually put into consideration during the design. The loading situations give rise to fatigue as the dominating mode of structural failure and this is a major concern. The fatigue phenomenon is enhanced by the corrosion process in the offshore environment.

Typical fatigue loading histories on structures are diverse, ranging from simple to repetitive to completely random. In other words, real load conditions are complex. The loading may be quasi-stationary, periodic, stochastic or transient, varying in time and origin [76][78]. In fact, the stochastic nature of fatigue loading on WT structures is not easily defined [49]. The design of the support structure is fundamentally based on load assumptions and simplifications; the simplification permits numerical modelling and simulations [48]. For a design life of about 20 years, the structure is expected to withstand some 10^9 cycles of fatigue loading [48]. However, the design life and number of cycles the structure of a WT can sustain depends on the structural dimensions, soil-structure interaction, natural frequency, stiffness and damping, water depth, turbine size [47][77][79][80] and material properties of the support structures.

The overturning capacity under extreme conditions is basically what determines the length of a monopile support structure, or the maximum allowable tilt of the turbine over its life time due to accumulated rotations from cyclic loading [81]. The diameter of the monopile is typically driven by requirements for the natural frequency of the turbine, and the soil stiffness is an important factor that is strongly linked to the dimensions of the monopile [81]. Fatigue and shell buckling are the two fundamental parameters that determine the thickness of a WT structure. Fatigue is of most concern in the welded regions.

The common analytical equations often employed in the design of a WT support structure, especially the tower, are given in Table 6. It can be seen from these equations that the buckling and bending that must be designed against have a direct relation to the yield strength, diameter and thickness of the steel used for the support structure. Thus, the main concern is to ensure sufficient stiffness to withstand the dynamic force of wind and waves [59].

According to DNV Standard [82], tubular members with low D/t ratios are generally not subject to local buckling under axial compression and can be designed on the basis of material yielding. This simply means that the yield strength of the steel can be taken to equal the local buckling stress. If the ratio D/t increases, the elastic local buckling strength decreases, making local buckling checks necessary. In other words, for that simple ratio, increasing the thickness of the steel section eliminates elastic buckling tendencies. Increasing the thickness this way to check the buckling of XL monopiles has a severe penalty that must be paid in terms of the structural integrity of the thick steel section.

7. Selection of strengthening mechanism for fatigue resistance of support structure of large wind turbine

The aim of the fatigue design of a WT is to ensure that it has adequate cyclic life. Calculated fatigue lives also form the basis for efficient inspection programs during fabrication and the operational life of the structure. DNV-RP-C203 [83] recommends the use of *fatigue tests* and *fracture mechanics* for fatigue analyses of WT structures.

Potential fatigue crack could come from welded joints, points of change in geometry, and from other parts of the structure, requiring fatigue analysis to be extended to all parts of the structure or component. In welded joints, fatigue cracks may start and grow from the weld toe, weld end, HAZ, weld root or even at weld metal.
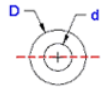
The fatigue strength of welded joints is found to depend to some extent on plate thickness. This effect is said to be due to the local geometry of the weld toe in relation to the thickness of the adjoining plates. It is also dependent on the stress gradient over the thickness. To account for the thickness effect on fatigue, a modification to the stress is made such that the design S-N curve for thickness other than the reference thickness reads [[83]; pp. 17-18]:

$$\log N = \log \bar{a} - m \log \left[\Delta\sigma \left(\frac{t}{t_{ref}} \right)^k \right]$$

where m is the negative inverse slope of the S-N curve; $\log \bar{a}$ the intercept of the $\log \bar{N}$ axis; t_{ref} is the reference thickness which equals 32mm for welded tubular joints, 25mm for bolts, t is the thickness through which a crack will most likely grow; and k the thickness exponent of fatigue strength. Again, it can be seen from this equation that the number of cycles to failure depends on the stress range and section thickness of the steel. According to the equation, as thickness increases the number of cycles to failure decreases.

Of particular interest for the design of new generation large WTs in the marine environment is the steel sub-grades listed in Table 5. They are commonly produced by Dillinger Hütte, Tata Steel or ArcelorMittal, certified by either Lloyds Register of Shipping (LRS) or DNV (Det Norske Veritas), depending on the thickness, and supplied as a hot rolled plate with thickness up to 100mm. Thickness of this magnitude invariably increases the scale of defects – inclusions and segregations (brittle zones) – thereby decreasing the integrity of such a structure.

Table 6: Common analytical expressions for the design of a wind turbine support structure, especially the tower [35] [76][83][84][85][86]

Parameter	Equation
Area moment of inertia (or second moment of area), $I_{tower} (m^4)$	$I = \dfrac{\pi}{64}(D^4 - d^4)$ D = outside diameter of the tower d = inner diameter of the tower
Radius of gyration $r_g\ (m^2)$	$r_g = \dfrac{1}{4}\sqrt{D^2 + d^2}$
Torsional stiffness constant $K(m^4)$	$K = \dfrac{\pi}{32}(D^4 - d^4)$
Cross-sectional area of the conical tower, $A\ (m^2)$	$A = \dfrac{\pi}{4}(D^2 - d^2)$
Mass per length, $m (kg/m)$ (where ρ is the mass density)	$m = A\rho$

(a) Geometrical parameter calculations

Parameter	Equation
2. Bending check	
$f_b = \dfrac{M}{Z_e} \leq \dfrac{F_b}{\gamma_{R,b}}$	f_b = bending stress due to forces from factored actions $\gamma_{R,b}$ = partial resistance factor for brnding strength M = bending moment due to factored actions F_b = representative bending strength $F_b = \left(\dfrac{Z_p}{Z_e}\right)F_y \quad for \quad \dfrac{F_y D}{Et} \leq 0.0517$ $F_b = \left[1.13 - 2.58\left(\dfrac{F_y D}{Et}\right)\right]\left(\dfrac{Z_p}{Z_e}\right)F_y \quad for\ 0.0517 < \dfrac{F_y D}{Et} \leq 0.1034$ $F_b = \left[0.94 - 0.76\left(\dfrac{F_y D}{Et}\right)\right]\left(\dfrac{Z_p}{Z_e}\right)F_y \quad for\ 0.1034 < \dfrac{F_y D}{Et} \leq 120\dfrac{F_y}{E}$ Z_e = elastic section modulus $Z_e = \dfrac{\pi}{32}\dfrac{[D^4 - (D - 2t)^4]}{D}$ Z_p = plastic section modulus $Z_e = \dfrac{1}{6}[D^3 - (D - 2t)^3]$

(b) Bending calculations

Parameter	Equation
1. Axial compression and buckling strength	
$f_c \leq \dfrac{F_c}{\gamma_{R,c}}$	f_c = axial compressive stress due to forces from factored actions F_c = representative axial compressive strength $F_c = [1.0 - 0.278\lambda^2]F_{yc}, \quad for\ \lambda \leq 1.34$ $F_c = \left(\dfrac{0.9}{\lambda^2}\right)F_{yc}, \quad for\ \lambda > 1.34$ $\lambda = \dfrac{KL}{\pi r_g}\sqrt{\dfrac{F_{yc}}{E}}$ $\gamma_{R,c}$ = partial resistance factor for axial compressive strength (= 1.18) E = Modulus of elasticity λ = column slenderness parameter K = effective length factor F_{yc} = representative local buckling strength $F_{yc} = F_y \quad for\ \dfrac{F_y}{F_{xe}} \leq 0.17$ $F_{yc} = \left[1.047 - 0.274\dfrac{F_y}{F_{xe}}\right]F_y \quad for\ \dfrac{F_y}{F_{xe}} > 0.17$ $F_{xe} = \dfrac{2C_x Et}{D}$ F_y = representative yield strength F_{xe} = representative elastic local buckling strength C_x = critical elastic buckling coefficient = 0.3 t = wall thickness of the tower
$N_{sd} \leq Af_c$	N_{sd} = design axial force

(c) Compression and buckling strength calculations

The ideal structural steel combines high strength with excellent fracture toughness. The strength of steel microstructures is commonly factorized into a number of intrinsic components [87]:

$$\sigma = \sigma_{Fe} + \sum_i x_i \sigma SS_i + x_C \sigma_C + K_L\{L\} + K_D \rho_D^{0.5}$$

where σ_{Fe} is the strength of pure annealed iron, 219MPa (MNm^{-2}) at temperature of 27°C; x_i is the concentration of a substitutional solute which is denoted here by a subscript i; σ_{SS_i} is substitutional solute (i) strengthening; σ_C is solid solution strengthening due to carbon; $K_L\{L\}$ is the function for strengthening due to 'grain' size, given as 115 (MNm^{-1}); K_D is the coefficient for strengthening due to dislocations, 7.34 $\times$ 10^{-6}MNm^{-1}; ρ_D is dislocation density, typically 10^{16} m^{-2}; and L is the measure of the ferrite plate size, typically 0.2µm.

The reduced alloying-element contents, including carbon of M-series steel sub-grades in Table 5, are expected to give the steel high weldability. This property will be good for thick shell sections in large WT design. For non-tempering steel, the increase in the strength of the steel can be achieved by solid-solution alloying, strain hardening and grain-size reduction. Note that the dispersion-strengthening process is utilized for tempered steels. The reduced alloying elements in these steels will tend to reduce the strength of the steel due to reduction in the strength contributions from solid solution – substitutional (such as Mn, Cr, Mo, etc.) and interstitial (carbon). Again, the M-series are supposed to be hot-worked in an austenite range and essentially there is little or no strain-hardening strengthening contribution in hot-worked steel. To make up for this, other strengthening methods need to be adopted, one of which is grain refinement. It is well established that fine grained microstructure in a steel can confer high mechanical strength and toughness [88]. In other words, decreasing the grain size can increase both the strength and the toughness of a steel simultaneously [89]. A typical plot illustrating the effect of grain refinement on a mild steel is shown in **Error! Reference source not found.**. In Fig. 8, decrease in D increases the flow stress.
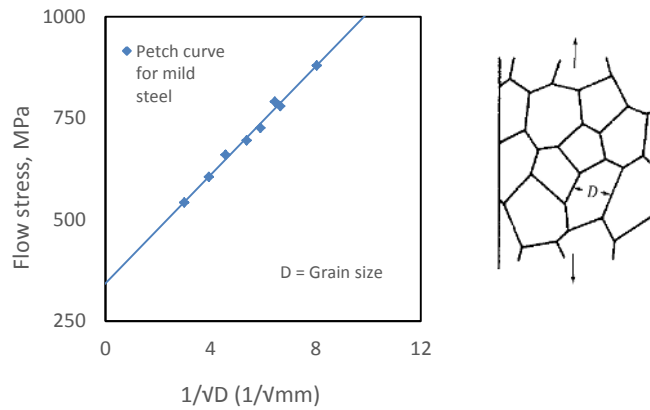

Fig. 8: The increase in strength with grain size reduction (Adapted from [90][91]).

This strength variation with grain size, at ambient temperature is usually expressed by the Hall-Petch relationship of a polycrystalline material as given in equations 1, 2 and 3.

$$\sigma = \sigma_o + kD^{-0.5} \qquad \text{Equation 1}$$
$$\sigma_y = \sigma_{oy} + k_y D^{-0.5} \qquad \text{Equation 2}$$
$$\sigma_F = \sigma_{oF} + k_F D^{-0.5} \qquad \text{Equation 3}$$

where σ is the yield (or flow) stress; σ_o is the friction resistance for dislocation movement within the polycrystalline grains or simply the friction stress denoting the total resistance of the crystal lattice to movement of dislocation; and k is a measure of the local stress needed at a grain boundary to move the dislocation. If the flow is plastic, it is denoted as k_y or k_c if the flow or fracturing is by cleavage at a lower

temperature. In other words, k is a parameter that measures the relative hardening contribution (dislocation locking) of the grain boundary. D is the average polycrystal grain diameter [90][91][92]. The value of σ_o is not the same for yielding and cleavage. σ_o, k_y and k_c are constants for a particular material.

This equation was proposed by Hall [92] and extensively expanded by Petch [93][94]. The Hall-Petch equation has been found to express the variation of brittle fracture stress with grain size and the dependence of fatigue strength on grain size. Yield stress, σ_y, and the "fatigue limit", σ_F depend on steel grain size, D as expressed in equations 2 and 3 respectively [90][95].

This dependence is reported to vary according to whether the fatigue stress is greater than, equal to, or less than the yield stress of the same material for low-carbon steel [96]. The increase in fracture toughness with reduction in grain size as composition and other microstructural variables are kept constant, is shown in Fig. 9. The fracture toughness K_c value usually increases with reduction in grain size as composition and other microstructural variables are kept constant. The fine grain size helps to minimize dislocation pile ups stresses.
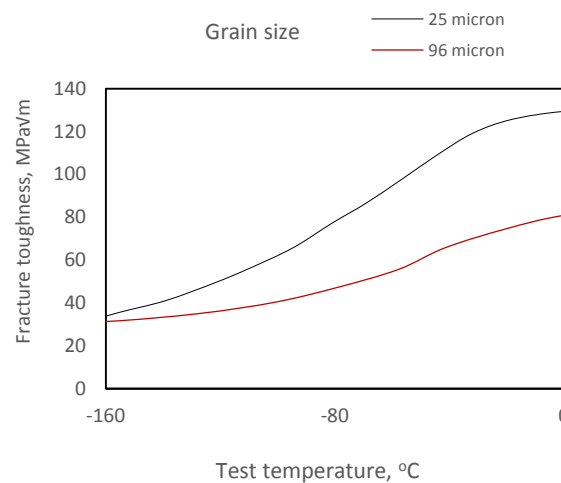

Fig. 9: Effect of grain size on fracture toughness of St37-3 steel (Adapted from [97]).

The Hall-Petch equation has also been found to apply to other kinds of boundaries, such as ferrite-cementite in pearlite, mechanical twins, and martensite plates. As already noted, a finer grain structure provides higher strength and ductility. This strengthening mechanism is unique, in the sense that other strengthening techniques give increased strength but with a corresponding reduction in toughness. Strengthening by finer grain size is achieved, in part, by the increase in the number of grain-boundary regions as the grain size is reduced. As the grains become finer, the grain boundary area impeding dislocation movement increases.

Grain boundaries are stronger than individual grains at temperatures below an equicohesive temperature. Equicohesive temperature is the temperature below which grain boundaries become stronger than the crystalline grains, or above which grain boundaries become weaker than the grains. Moreover, because a greater number of randomly aligned grains are achieved when grain size is reduced, the stressed material has more opportunity to allow slip and thus improve ductility. In contrast, coarser-grained material tends to exhibit generally poorer mechanical properties, e.g. lower yield strength, higher ductile-brittle transition temperature, and poorer long-life fatigue properties. Thus, as already noted, grain size refinement provides a means for the materials engineer to increase both strength and ductility (toughness) [98]. Hence, strength, including long-life fatigue strength, DBTT, fracture toughness and hardness directly or indirectly depend on grain size, and the dependence is strong enough that commercial mechanical/thermal processing practice is focused on keeping the grain size as small as possible. However, it has been reported that excessive grain refinement to raise yield strength is limited by the onset of grain boundary sliding in the fine-grained microstructure [99].

8. Thermomechanical processing of *M-series* steel sub-grades

As already discussed, exceptional strength-toughness combinations can be achieved in even low-alloy steels by refining grain size. TMCP is a manufacturing method through which this kind of grain refinement is achieved. The process is essentially a combination of controlled rolling and controlled cooling operations. Fig. 10 presents typical inline methods for cooling hot rolled steel superimposed on a continuous cooling temperature (CCT) diagram. The austenitization is done such that grain growth is suppressed. In the rough rolling stand, recrystallization (strain-free grains with low density of dislocations) takes place and deformed recrystallized grain is obtained in the finishing stand. If the cooling is fast, martensite forms in sufficiently alloyed steel. If moderately cooled, bainite forms, while ferrite and pearlite forms when slow cooling is obtained [72]. The strength of the steel increases from slow cooling to accelerated cooling. The superior point of this process is that high tensile strength can still be obtained with a reduction in the amount of carbon and other alloying elements, as is the case for the M-series steel in Table 5.
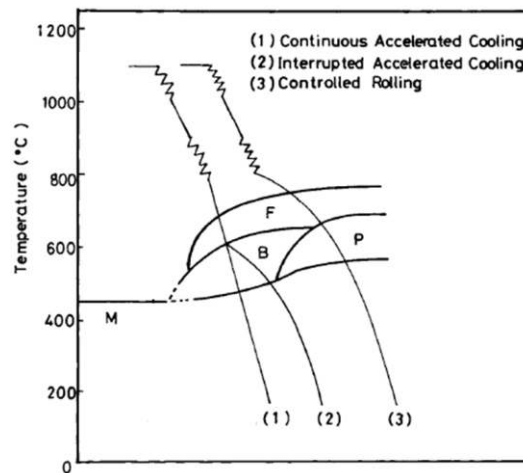

Fig. 10: Typical methods of inline cooling after hot-rolling for TMCP steel.

The low carbon equivalent (C_{eq}) and fine grains confer two major advantages; very good weldability and improved toughness. The superiority of this process in terms of tensile strength is shown in Fig. 11. TMCP steel gave the highest tensile strength at all carbon equivalents. Hence, the overall essence of thermomechanical processing is to produce the finest possible grain in other to achieve the end results by combining plastic deformation (which is necessary to shape the steel) with controlled heat treatment to give recrystallized grains.
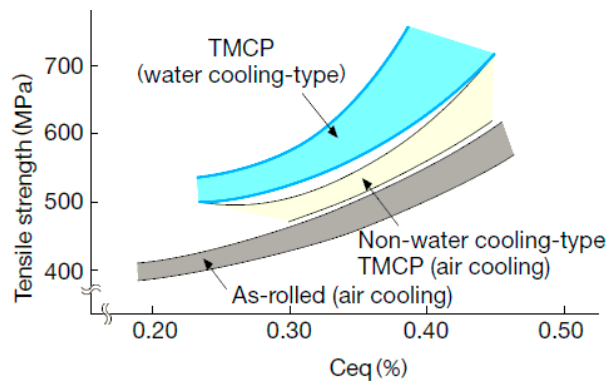

Fig. 11: Comparison of TMCP and conventional process, in terms of tensile strength and C_{eq} for plate thickness of 20 to 30mm [72].

There are limits to the smallest grain size that can be obtained by applying the theory of phase transformation in steel. Theory has shown that a grain size of allotriomorphic ferrite much smaller than 1μm is unlikely in large-scale production processes [100]. In conventional controlled rolling, 5μm is reported to be achievable by the transformation of deformed austenite grains to ferrite due to generation of a greater

number of nucleation sites in the rolled (pancake-like) austenite. It has been found that the Hall-Petch relation correlates well with experimental results on many metals and alloys, but tends to be invalid for a low strain rate, coarse and very fine grain sizes [101].

A major barrier to the successful implementation of thermomechanical processing on thick plates is that it is difficult to impart large, uniform deformation through the thickness of plate steel [99]. To obtain fine grain size high rolling deformation (80% or more) is required and since the whole thickness will not be rolled, care must be taken not to assume that uniform property exists within the material. Hence, we may have an inner core that has grain growth which is detrimental to fatigue life – particularly crack initiation.

9. Structural metallurgy and integrity of thick TMCP steels for the support structure of XL-WTs

9.1   The effect of temperature

Temperature is one of the most important external variables that influence the mechanical behavior of steel. The three basic crystal patterns associated with metals are: (a) the body-centered cubic (*bcc*), (b) the face-centered cubic (*fcc*) and (c) the hexagonal close-packed (*hcp*). Iron or ferrite has a *bcc* structure while austenite is *fcc*. The interstitial solid solution of carbon in *γ-Fe* is called *austenite* (*γ*). Temperature dependence of the mechanical properties is found to vary for *bcc* and *fcc* crystal structures of steels. The *fcc* phase (austenite) commonly exhibits plastic deformation and ductile fracture mechanisms, even at low temperature, but *bcc* (ferrite) undergoes cleavage fracture at low temperatures. This temperature effect is commonly illustrated as shown in Fig. 12.
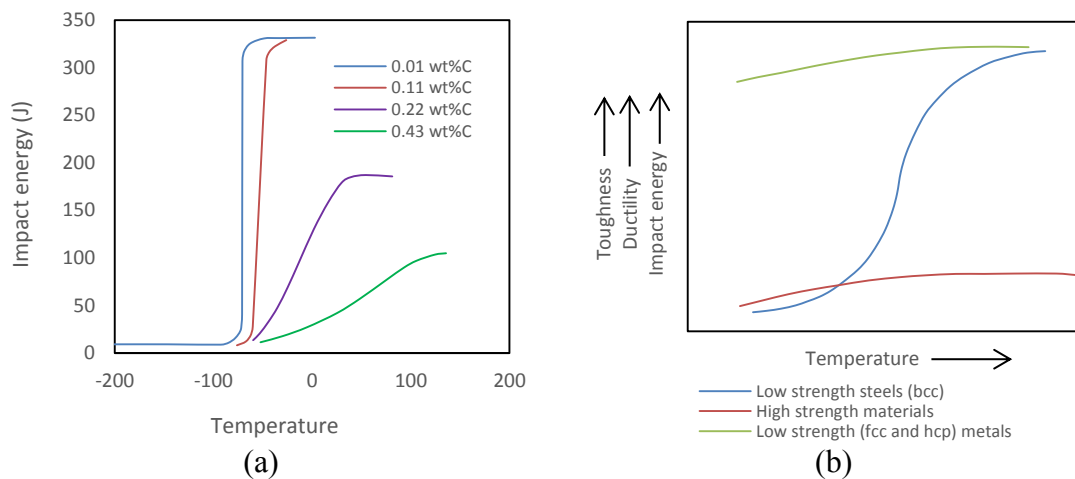

Fig. 12: (a) Effect of increasing carbon content of steel on the Charpy V-notch energy vs. temperature curve. (b) Effect of temperature on toughness and ductility of *fcc*, *bcc*, and *hcp* metals (Adapted from [102])

The reduced carbon content in M-series steels (Table 5) will decrease the transition temperature as can be seen in Fig. 12 (a). Also another advantage of finer grain size is the decrease in the transition temperature [99]. Increase in grain diameter raises the DBTT and this trend is usually observed for increases in loading rate [93][98] .

Decreasing grain size and carbon content both decrease the ductile to brittle transition temperature. This is where M-series steel sub-grades seems to be superior as they may not suffer from this kind of CVN transition shift due to their low alloying contents and finer grain size. However, as the volume fraction of ferrite (*bcc*) increases due to reduction of carbon, there may be a competing process making ductile to brittle fracture a serious concern.

17

9.2   The effect of plate thickness

The plate thickness is another important factor in the brittle-ductile transition problem. This effect is commonly associated with the size of the deformation zone in comparison with the plate thickness. It is found that the transition temperature shifts to the left for thin plates. In other words, thick plates are more brittle than thin ones at low temperatures. Plane strain condition, associated with an increase in sample thickness imposes a more significant plastic constraint on the plastic zone than does plane stress. The triaxial stress field that exists in thick plates tends to decrease the extent of plastic deformation, thereby increasing local stresses which could lead to brittle failure.

It is practically impossible to obtain uniform fine grains across the thickness of a thick plate (or what the authors may refer to as XL steel plates) due to recalescence (liberation of the enthalpy of transformation or latent heat of transformation) [100]. The beneficial mechanical disruption or breakup of non-metallic inclusions and grain refinement during rolling does not occur to the same extent for both the outer regions and inner region of the steel during metalworking. Hence, the fatigue property of thick TMCP steels is not expected to be the same across the thickness of the material – in fact the so-called fine-grained structure may only be obtained at a shallow depth from the metal surface and the interior, which is practically unaffected by the TMCP process, may have significant implications for the design of XL-WTs where an increase in section thickness is used to achieve high stiffness and buckling strengths.

Typical microstructures in a hot rolled, low-alloy steels are shown in **Error! Reference source not found.**. **Error! Reference source not found.**(a & c) are microstructures of S355J2+N [103], **Error! Reference source not found.**(b) S355 (sub-grade unspecified) [104] with composition as shown in Table 7. **Error! Reference source not found.**(c) shows the inherent segregation associated with hot rolled ferritic steels. **Error! Reference source not found.**(e & f) are the microstructures of S355G8+M and S355G10+M respectively.
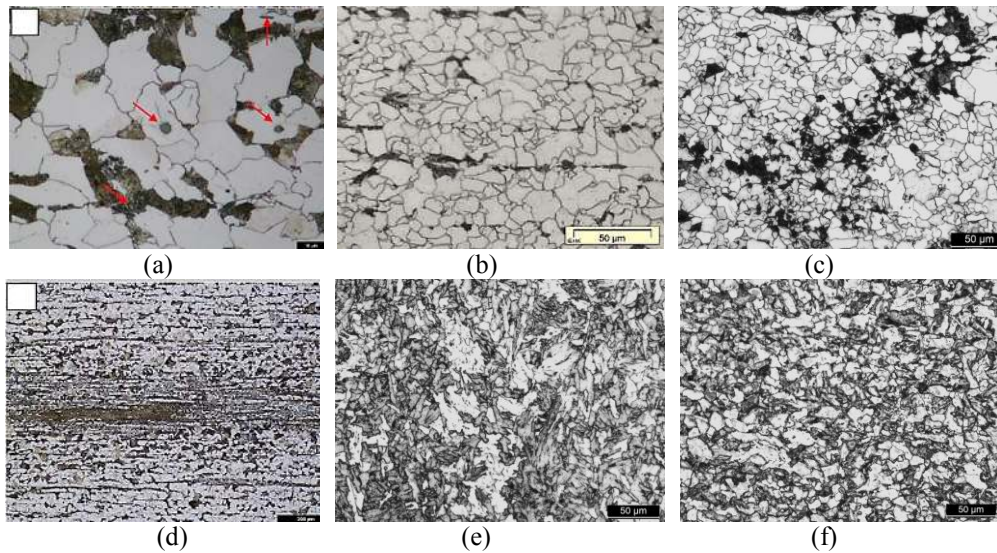

Fig. 13: Typical microstructures of hot rolled low-alloy steels: (a) S355J2+N [103], (b) S355 (grade unspecified) [104], (c) S355J2+N, (f) segregation associated with hot rolled S355J2+N steel [103], (e) and (f) are the microstructures of S355G8+M and S355G10+M respectively:

A microstructural examination of S355J2+N with properties as shown in Table 7, shows that 80% of the microstructure is allotriomorphic ferrite and others pearlite, with traces of acicular or Widmanstätten ferrite [103]. Hardness is around $168HV_{0.1}$ with equiaxed grains of average size of 15μm, measured in the through-

thickness direction. The arrows in **Error! Reference source not found.**(a) are some inclusion such as MnS [104]. **Error! Reference source not found.**(b - c) confirms that S355 steel is predominantly ferritic. **Error! Reference source not found.**(d) is the alignment of pearlite in the rolling plane, which is often referred to as microstructural banding. The banding is commonly more evident in sections containing the rolling direction than in those containing the transverse direction [105][106]. Banding can also be attributed to segregation of solutes in the last regions of the steel melt to solidify during the cooling of steel from the molten state. In low-carbon/low-alloy steels prone to banding, solidification starts as δ – ferrite. As the volume fraction of this delta phase increases, solutes such as Mn, Si, P and S partition into the interdendritic regions, which then solidify later with a higher than average concentration of these solutes [107]. Successive deformation during the hot rolling causes these regions to spread out as bands. The pearlite and ferrite in this segregation zone are usually harder and may extend up to 400µm [103]. Since other alloying elements are relatively very low in M-series steels, the segregation of concern will be mainly that of Mn – a substitutional element, although other solutes such as Ni, Cr, Si can be found in the pearlite band phase [106]. The presence of unbroken segregation zones in the inner material of thick plates, which increase with plate thickness, may impact negatively on the toughness of the support structure of a WT made with XL steel plates. Micrographs of **Error! Reference source not found.** (c), (e) and (f) are part of an ongoing project by the authors to ascertain the integrity of S355 thick plate subgrades.

Table 7: Properties of steels whose microstructures are shown in **Error! Reference source not found.**.

S355J2+N Chemical composition		**CHEMICAL COMPOSITION OF S355 STUDIED**	
C	0.22	C	0.054
Si	0.55	SI	0.018
Mn	1.60	MN	1.085
P	0.035	P	0.011
S	0.035	S	<0.001
Cr	0.30	CR	0.015
Mo	0.08	MO	<0.005
Ni	0.30	NI	0.019
Al	0.02	AL	0.021
Cu	0.55	NB	0.023
		CU	0.010
		TI	0.009

The separation of ferrite and pearlite phases into bands creates local microstructural properties. The presence of a hard phase in a soft matrix is expected to influence fatigue crack growth behavior in the steel. The difference in local properties due to two different phases with dissimilar stiffnesses would affect the fatigue crack growth behavior of the material. A study found that banding, often seen in hot rolled steel plates, contributes to a superior fatigue strength and higher threshold values [108]. The orientation of the pearlite banding in the studied steel was seen to offer higher resistance to fatigue crack growth [108]. The pearlite band, which is the hard phase, was reported to be responsible for arresting and deviating the crack propagation [108], as shown in Fig. 14(a &b).
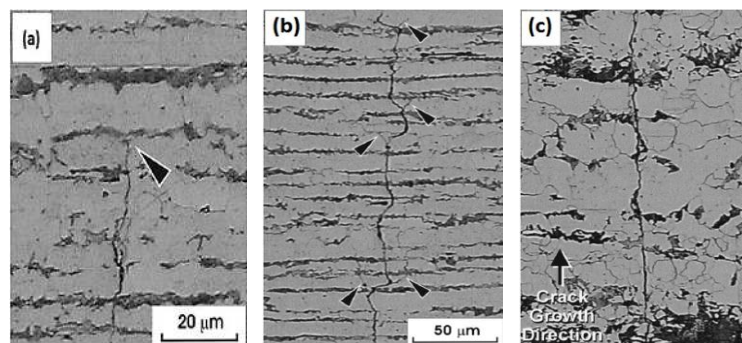
The arrow shows where the crack tip was arrested in Fig. 14(a), and the near-threshold region crack branching in Fig. 14(b). The crack branching was reported to occur after passage of the crack tip through the pearlite band [108]. It was also reported that the extensive crack branching reduced the fatigue crack propagation driving force at the local crack tip. This effect of banding for hot rolled plate may possibly be seen on the outer region of XL steel plates while the inner material is essentially non-banded. In fact, XL steel plates are not expected to be banded, as can be seen from **Error! Reference source not found.**(d) and (e). The microstructures of these ferritic-pearlitic TMCP steels are clearly different and the comparative fatigue crack growth resistance performance study with normalized subgrades have not been carried out or the data are very scarce.

9.3   Potential challenges in welding thick plates

As already noted, coarse-grained material tends to exhibit generally poorer mechanical properties, e.g. lower yield strength, higher ductile-brittle transition temperature, and poorer long-life fatigue properties. Decreasing grain size and carbon content both decrease the ductile to brittle transition temperature and increase both the strength and toughness of a steel simultaneously. When these steels are welded, the benefits of the much-celebrated thermo-mechanical processing are lost. Fine-grain pearlite microstructure is tolerant of weld defects. Pearlite is composed largely of the ductile ferrite phase containing about 13% by volume of the hard intermetallic compound, cementite [97]. Fine pearlite is found to offer highest resistance to crack initiation under high cycle fatigue conditions; this finding was attributed to the formation of a more homogeneous distribution of plastic strain in fine pearlite than in a coarse one [109]. The cycling associated with multiple weld passes can cause the formation of coarse pearlite which tends to reduce the fracture toughness of the material.

Residual stress has been defined as that stress which remains in a body that is stationary and at equilibrium with its surroundings [110]. Development of residual stresses after welding occurs due to localized heating/fusion and non-uniform application of heat energy (sharp thermal gradient). As the weld pool is solidifying it thermally contracts and exerts a pull on the surrounding material and this pull places the region under tensile stress, as shown in Fig. 15. The thermal contraction of the weld metal may be too large to sustain elastically, causing plastic deformation to occur [111]. Having many phases in a microstructure or phase transformation can cause grain scale stresses to exist in a material [110]. If microstructural transformation effects are neglected, significant tensile stresses remain in the near weld region when the welding operation is completed and thermal equilibrium reached by the component.

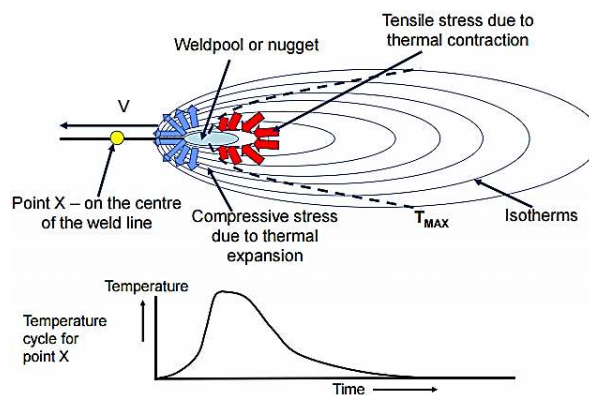Fig. 15: Schematic of development of tensile residual stress during fusion welding [112].

Residual stresses are essentially not a part of a material and not needed to maintain equilibrium. They exist as a result of human handling of the material. It has been reported that tensile residual stresses after welding can contribute to fatigue crack development in a structure, even under compressive cyclic loading

[113][114]. The tensile residual stress could combine with the service stresses, increasing the mean stress and this seriously reduces the lifespan of structures. Hence, residual stress is very detrimental to the fatigue performance of a steel, or the life of a component.

9.4   Change in the weld metallurgy

During fusion welding the heat generated is conducted away by the parent metal. The rate of heat conduction affects the weld metallurgy. **Error! Reference source not found.** is a weld schematic showing various local regions for a single pass weld. The heat affected zone (HAZ) is an area in the material that is not heated high enough to cause melting, but its microstructure is altered by the thermal cycling during welding. It lies immediately after the fusion zone.
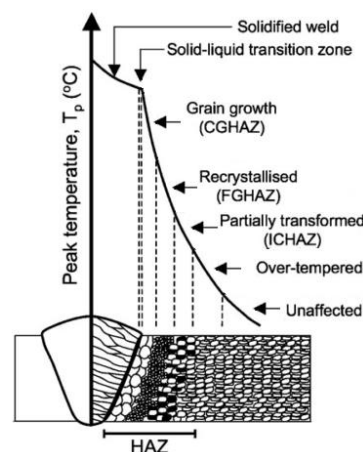

Fig. 16: Weld metallurgical zones in a single pass weld [107] (see also [115][116])

The HAZ is commonly subdivided into coarse-grained (CG) – region of grain growth; fine-grained (FG) – region of recrystallized grain; inter-critical (IC) – region of partially microstructural transformation; and over-tempered (OT) – region of over tempering on the parent metal. This classification is based on the extent to which grain growth and austenitization occur. To weld thick walled plates, as would be required for modern WT support structures, many welding passes are needed to fill the joint. During the process, the previous weld beads would experience reheating due to deposition of succeeding beads causing the metallurgical zones to be further subdivided.

The CGHAZ zone is associated with reduction in toughness. Reheating due to multi-pass welding at the region of coarse-grained HAZ could make worse the decline in toughness [117][118]. The constant re-austenitization of certain portions of the weld due to the multiple passes could result in segregation of alloying elements (e.g. C, Mn, Ni, Co,) in steels containing them. The effect of this upon cooling is the formation of local regions that have transformed into hard microstructures, which is detrimental to toughness. These regions are often called local brittle zones.

For XL plates, filler rods with a different composition to that of the parent metal are often used. In a multipass weld, the composition of a previous weld bead can vary from the succeeding weld bead as a result of changes in dilution levels. The resultant weld microstructure is a function of the degree of dilution, which depends on the extent of variation in composition between the filler metal and parent metal. Weld dilution has been found to be detrimental to weld toughness [46][119]. The microstructure at the surface of the structural material influences considerably the fatigue properties [101] and in a corrosive environment this surface is under attack.

Failure during WT service is accompanied by huge economic cost. The need to select the right material cannot be overemphasized in order to reduce capital expenditure (CAPEX) and in-service fatigue failure. Thus, a reliable fatigue study of all sub-grades of S355 – normalized and TMCP steel – in a marine environment must consider the effect of plate thickness, frequency, waveform and corrosion. Hence, research is currently ongoing to provide the fatigue crack growth rates, guidance on inspection requirements and prediction of corrosion fatigue life of offshore structures designed with ferritic steels, with the focus on comparing normalized and TMCP S355 steels.

10. Conclusions

Some of the findings and structural integrity issues raised in this paper can be summarized thus:

1. All indications show that the global energy from wind power will rise due to rapid reduction in the cost of wind energy. With advances in turbine technology, efficient and optimized turbine support structure the outlook shows that wind energy will become the major and critical renewable source of electricity in the UK by end of 2030.

2. TMCP steels are reported to be well situated for XL-WTs. The reduced alloying-elements in this steel will give the steel high weldability and this property will be good for thick sections in XL-WT design. The reduced alloying elements in these steels will tend to reduce the strength of the steel due to reduction in the strength contributions from solid solution. M-series are supposed to be hot-worked in an austenite range and essentially there is little or no strain-hardening strengthening contribution in hot-worked steel. Hence, grain refinement remains the best strengthening method for this steel to attain high mechanical strength and toughness. In general, the low carbon equivalent (C_{eq}) and fine grains confer two major advantages; very good weldability and improved toughness.

3. A major barrier to the successful implementation of thermomechanical processing on thick plates is that it is difficult to obtain large, uniform deformation through the thickness of plate steel. To obtain fine grain size, high rolling deformation (80% or more) is required. Thus, for M-series only a small zone is probably rolled and care must be taken not to assume that uniform property exists within the material. It is likely we will have an inner core that has grain growth which reduces fatigue life. The advantage of this M-series sub-grade of S355 and that of normalized S355 of similar composition in terms of corrosion fatigue needs to be critically assessed to aid economic material selection decisions and use of steels for various engineering applications in marine environment.

4. Decreasing grain size and carbon content both decrease the ductile to brittle transition temperature. However, as the volume fraction of ferrite (*bcc*) increases due to the reduction of carbon, there may be a competing process making ductile to brittle fracture a serious concern.

5. Increasing the thickness of the steel section eliminates elastic buckling tendencies. Increasing the thickness this way to check buckling of XL monopiles has a severe penalty that must be paid in terms of structural integrity of the thick steel section.

6. Plane strain condition, associated with an increase in sample thickness, imposes significant plastic constraint on the plastic zone than does plane stress. The triaxial stress field that exists in thick plates tends to decrease the extent of plastic deformation, thereby increasing local stresses which could lead to brittle failure. Hence, thick plates are more brittle than thin plates.

7. It is practically impossible to obtain uniform fine grains across the thickness of XL steel plate due to recalescence. The beneficial mechanical breakup of non-metallic inclusions and grain refinement during rolling for XL plates merely occurs at a small layer on the metal surface. Consequently, the fatigue property of TMCP steels is not the same across the thickness of the material. The interior, which is practically unaffected by the TMCP process, may have experienced grain growth and segregations and this could have a negative impact on the toughness of the support structure of XL-WTs, where an increase in section thickness is used to achieve high stiffness and buckling strengths.

8. The design S-N curve, such as given below, shows that as thickness increases the number of cycles to failure decreases exponentially if other variables remain constant.

$$\log N = \log \bar{a} - m \log \left[\Delta\sigma \left(\frac{t}{t_{ref}}\right)^k\right] \qquad \text{Equation 4}$$

9. It is likely that the large scale of defects, inclusions, grain growth and segregation (brittle zones) accompanying an increase in thickness could accelerate crack propagation in the inner material of XL-WT support structures.

10. When these steels are welded, the benefits of much celebrated thermo-mechanical processing are lost. Fine pearlite is found to offer highest resistance to crack initiation under high cycle fatigue conditions. The cycling associated with multiple weld passes can cause the formation of coarse pearlite, which is detrimental to fracture toughness.

11. The development of residual stresses after welding occurs due to localized heating/fusion and non-uniform application of heat energy. To weld thick walled plates, as would be required for modern turbine towers, many welding passes are needed to fill the joint. If microstructural transformation effects are neglected, large tensile stresses could remain in the near weld region. The tensile residual stress is very detrimental to the fatigue performance of a steel. Tensile residual stress is reported to contribute to fatigue crack development in a structure, even under compressive cyclic loading.

12. Weld microstructure is a function of the extent of dilution by the filler metal. Weld dilution could be a problem with thick plates and is found to be detrimental to weld toughness.

13. The knowledge of temperature and corrosion effects, fatigue crack growth rate and magnitude of residual stress will enable cost effective design of next generation OWTs.

Finally, apart from consideration of the enumerated design factors, next generation OWT support structures should consider achieving buckling strength and required fatigue life through innovative increases in diameter, rather than thickness, in order to avoid some of these structural integrity concerns.

Acknowledgements

References

[1] EEA. Renewable energy in Europe – 2017: Recent growth and knock-on effects. 2017.

[2] Higgins P, Foley A. The evolution of offshore wind power in the united kingdom. Renew Sustain Energy Rev 2014;37:599–612. doi:10.1016/j.rser.2014.05.058.

[3] GOV.UK. The Clean Growth Strategy - leading the way to a low carbon future. 2017.

[4] Leanwind. Driving Cost Reductions in Offshore Wind. 2017.

[5] Smarter business. UK renewable energy percentage 2018 2018. https://smarterbusiness.co.uk/uk-renewable-energy-percentage-2018/ (accessed October 15, 2018).

[6] RenewableUK. Wind Energy 2016. http://www.renewableuk.com/en/renewable-energy/wind-energy/ (accessed March 20, 2016).

[7] Luke Clark. UK Offshore wind capacity set to double following Government announcement. RenewableUK 2018. https://www.renewableuk.com/news/410144/UK-Offshore-wind-capacity-set-to-double-following-Government-announcement-.htm (accessed August 31, 2018).

[8] MyGridGB – Charting British electricity. September 2018. http://www.mygridgb.co.uk/ (accessed September 3, 2018).

[9] BEIS. PRESS NOTICE - UK Energy Statistics, 2017 Q4 2017. 2018.

[10] The Crown Estate. Offshore wind 2018:1–5. https://www.thecrownestate.co.uk/en-gb/media-and-insights/seabed-notices/offshore-wind/ (accessed October 19, 2018).

[11] Ecotricity. Our Fuel Mix. Ecotricity 2018. https://www.ecotricity.co.uk/our-green-energy/energy-independence/our-fuel-mix (accessed October 20, 2018).

[12] Beiter P et. al. 2017 Offshore Wind Technologies Market Update. 2017.

[13] Global Wind Energy Council. Offshore wind power 2017. http://gwec.net/global-figures/global-offshore/ (accessed September 1, 2018).

[14] The Crown Estate. Performance: Markets and portfolio review, in Integrated Annual Report and Accounts. 2018.

[15] BEIS. Contracts for Difference Second Allocation Round Results. 2017.

[16] E. Lantz et al. IEA Wind Task 26: The past and future cost of wind energy. Wind Energy 2012:1–126.

[17] Ahn D, Shin SC, Kim SY, Kharoufi H, Kim HC. Comparative evaluation of different offshore wind turbine installation vessels for Korean west–south wind farm. Int J Nav Archit Ocean Eng 2017;9:45–54. doi:10.1016/j.ijnaoe.2016.07.004.

[18] Windpower. Ten of the biggest wind turbines. Wind Mon 2018. https://www.windpowermonthly.com/10-biggest-turbines (accessed October 16, 2018).

[19] Power-technology.com. The world's 10 biggest wind turbines 2014. http://www.power-technology.com/features/featurethe-worlds-biggest-wind-turbines-4154395/ (accessed April 9, 2016).

[20] Whitby M. V164-8.0 MW® breaks world record for wind energy production. Denmark: 2015.

[21] Offshorewinduk. A History of Offshore Wind Power 2016. http://offshorewind.works/inform/a-history-of-offshore-wind-power/ (accessed March 28, 2016).

[22] 4COffshore. V164-8.0 MW 2016. http://www.4coffshore.com/windfarms/turbine-mhi-vestas-offshore-wind-v164-8.0-mw-tid89.html (accessed March 28, 2016).

[23] WindPower. The 10 biggest turbines in the world 2016. http://www.windpowermonthly.com/10-biggest-turbines (accessed April 10, 2016).

[24] Windpower. GE unveils 12MW offshore turbine. Wind Mon 2018. https://www.windpoweroffshore.com/article/1458364/ge-unveils-12mw-offshore-turbine-updated (accessed October 16, 2018).

[25] Baraniuk C. Reaping the wind with the biggest turbines ever made. BBC News 2018:1–12. https://www.bbc.co.uk/news/business-43576226 (accessed June 21, 2018).

[26] C. Bak et al. Description of the DTU 10 MW Reference Wind Turbine. Denmark: 2013.

[27] Gupta A. The world's 10 biggest wind turbines. Power Technol 2014. https://www.power-technology.com/features/featurethe-worlds-biggest-wind-turbines-4154395/ (accessed October 20, 2018).

[28] AMSC. SeaTitan 10 MW Wind Turbine 2012:2.

[29] H. Polinder et al. 10 MW wind turbine direct-drive generator design with pitch or active speed stall control. Proc IEEE Int Electr Mach Drives Conf IEMDC 2007 2007;2:1390–5. doi:10.1109/IEMDC.2007.383632.

[30] Frøyd L, Dahlhaug OG. Rotor Design for a 10 MW Offshore Wind Turbine. Int Offshore Polar Eng Conf 2011;8:327–34.

[31] 4Coffshore. SWAY 10 MW (onshore) test turbine offshore wind farm 2016. http://www.4coffshore.com/windfarms/SWAY-10MW-test-turbine-Norway-NO17.html (accessed April 9, 2016).

[32] S. Rodrigues et al. A Multi-Objective Optimization Framework for Offshore Wind Farm Layouts and Electric Infrastructures. Energies 2016;9:1–42. doi:10.3390/en9030216.

[33] 4Coffshore. Offshore Turbine Database 2016. http://www.4coffshore.com/windfarms/turbines.aspx (accessed March 27, 2016).

[34] Lindoe Offshore Renewables Center. LIST OF OFFSHORE WIND FARMS 2011. http://www.lorc.dk/offshore-wind-farms-map/list (accessed March 1, 2016).

[35] Bak C, Zahle F, Bitsche R, Yde A, Henriksen LC, Nata- A, et al. Description of the DTU 10 MW Reference Wind Turbine Department of Wind Energy I-Report. 2013.

[36] BEIS. UK Energy in Brief 2018. 2018.

[37] European Wind Energy Association. Deep water: the next step for offshore wind energy. 2013.

[38] Musial W, Beiter P, Schwabe P, Tian T, Stehly T, Spitsen P. 2016 Offshore Wind Technologies Market Report. US Dep Energy 2016:1–131. doi:DOE/GO-102017-5031.

[39] Caduff M, Huijbregts MAJ, Althaus HJ, Koehler A, Hellweg S. Wind power electricity: The bigger the turbine, the greener the electricity? Environ Sci Technol 2012;46:4725–33. doi:10.1021/es204108n.

[40] Kallehave D, Byrne BBW, LeBlanc Thilsted C, Mikkelsen KK, Association. EWE, Estate. TC, et al. Optimization of monopiles for offshore wind turbines. Philos Trans A Math Phys Eng Sci 2015;373:1–15. doi:10.1098/rsta.2014.0100.

[41] offshorewind. Offshore Wind Turbine Foundations- Current & Future Prototypes 2016. http://offshorewind.net/offshore-wind-turbine-foundations-current-future-prototypes/ (accessed April 17, 2016).

[42] JWPA. Offshore Wind Power Development in Japan. 2017.

[43] Offshore Wind. MHI Vestas Receives WindFloat Atlantic Order. Offshore Wind 2018. https://www.offshorewind.biz/2018/09/10/mhi-vestas-receives-windfloat-atlantic-order/ (accessed October 17, 2018).

[44] Floatgen. Floatgen has been inaugurated. Floatgen 2017. http://floatgen.eu/en/actualites/floatgen-has-been-inaugurated (accessed October 17, 2018).

[45] Atkins. Kincardine Floating Offshore Wind Farm n.d. https://www.atkinsglobal.com/en-gb/projects/kincardine-floating-offshore-wind-farm (accessed October 17, 2018).

[46] DOE & DOI. National Offshore Wind Strategy. 2016.

[47] Bhattacharya S, Nikitas N, Garnsey J, Alexander NA, Cox J, Lombardi D, et al. Observed dynamic soil-structure interaction in scale testing of offshore wind turbine foundations. Soil Dyn Earthq Eng 2013;54:47–60. doi:10.1016/j.soildyn.2013.07.012.

[48] Schaumann P, Steppeler S. Special fatigue aspects in support structures of offshore wind turbines 2011:1075–81. doi:10.1002/mawe.201100913.

[49] Brennan FP. A framework for variable amplitude corrosion fatigue materials tests for offshore wind steel support structures. Fatigue Fract Eng Mater Struct 2014;37:717–21. doi:10.1111/ffe.12184.

[50] Kallehave D, Byrne BW, LeBlanc Thilsted C, Mikkelsen KK. Optimization of monopiles for offshore wind turbines. Philos Trans A Math Phys Eng Sci 2015;373:1–15. doi:10.1098/rsta.2014.0100.

[51] 4Coffshore. Gemini Offshore Wind Farm. 4Coffshore 2016. http://www.4coffshore.com/windfarms/gemini-netherlands-nl18.html (accessed May 16, 2016).

[52] Sif-Group. XXL-monopiles by Sif Group for the Gemini Project. Sif Gr 2016. https://sif-group.com/en/news/15-xxl-monopiles-by-sif-group (accessed May 15, 2016).

[53] deBruin R. Van Oord installs Gemini wind project's first monopile. Van Oord 2016. http://www.vanoord.com/news/2015-van-oord-installs-gemini-wind-projects-first-monopile (accessed May 15, 2016).

[54] 4C Offshore. Gemini - 4C Offshore n.d. https://www.4coffshore.com/windfarms/gemini-netherlands-nl18.html (accessed June 23, 2018).

[55] Garus K. EEW has produced the world's heaviest Monopile. BVA Bielefelder Verlag GmbH Co KG 2016. http://www.offshorewindindustry.com/news/eew-produced-worlds-heaviest-monopile (accessed May 15, 2016).

[56] DONG-Energy. Gode Wind Offshore Wind Farm project. Dong Energy 2015. http://www.dongenergy.com/en/media/newsroom/news/articles/first-foundation-successfully-installed1.

[57] 4Coffshore. Burbo Bank Extension Offshore Wind Farm. 4Coffshore 2016. http://www.4coffshore.com/windfarms/burbo-bank-extension-united-kingdom-uk59.html (accessed May 16, 2016).

[58] University of Strathclyde. The Practicality and Challenges of Using XL Monopiles for Offshore Wind Turbine Substructures - Cost Analysis. 2015.

[59] Daubney K. IN DEPTH: Cost imperative drives monopiles to new depths. Wind Power Offshore 2013. http://www.windpoweroffshore.com/article/1210058/depth-cost-imperative-drives-monopiles-new-depths.

[60] U.S. Department of Energy. A National Offshore Wind Strategy: Creating an Offshore Wind Energy Industry in the United States. 2011.

[61] Mone C, Stehly T, Maples B, Settle E. 2014 Cost of Wind Energy Review. Natl Renew Energy Lab 2015.

[62] Hu Y, Baniotopoulos C, Yang J. Effect of internal stiffening rings and wall thickness on the structural response of steel wind turbine towers. Eng Struct 2014;81:148–61. doi:10.1016/j.engstruct.2014.09.015.

[63] Rivkin, D. A.,Toomey,K., Silk L. Wind Turbine Technology and Design. Burlington, UK: 2013.

[64] Nick Gillbert. Structural Steel - S235, S275, S355 Chemical Composition, Mechanical Properties and Common Applications 2012. http://www.azom.com/article.aspx?ArticleID=6022 (accessed July 30, 2016).

[65] Tata Steel. Advance sections. 2013.

[66] Steel International T. New Horizons - supply solutions in offshore structual steel. 2010.

[67] Corus Construction & Industrial. European structural steel standard EN 10025 : 2004. 2004.

[68] Parker Steel Company. S355 EN 10025: Standard Structural Steel Products 2012. http://www.metricmetal.com/products/Grade Descriptions/S355 Grade Description.php (accessed April 1, 2016).

[69] Ruukki. Hot-rolled steel plates, sheets and coils standard steel grades, comparison, designations and codes. 2011.

[70] Regency Steel Asia. EN 10225 Chemical & Mechanical Properties. 2016.

[71] Tata Steel International. Product range - global steel supply and services. 2010.

[72] Nippon Steel & Sumitomo Metal. Steel Plates for Offshore Structures. 2014.

[73] MEADinfo. Material Properties of S355 Steel - An Overview 2015. http://www.meadinfo.org/2015/08/s355-steel-properties.html (accessed April 11, 2016).

[74] Dillinger. Thermomechanically rolled fine-grained steels 2016. https://www.dillinger.de/d/en/products/heavyplate/thermomechanically-finegrained/ (accessed April 11, 2016).

[75] OAKLEY STEEL. S355G10+M TMCP OFFSHORE STEEL PLATES EN10225 2016. http://www.oakleysteel.co.uk/offshore-steel-plate/s355g10m-s355g10n (accessed April 11, 2016).

[76] DNV/Risø. Guidelines for design of wind turbines. 2002. doi:ISBN 87-550-2870-5.

[77] Lombardi D, Bhattacharya S, Muir Wood D. Dynamic soil-structure interaction of monopile supported wind turbines in cohesive soil. Soil Dyn Earthq Eng 2013;49:165–80. doi:10.1016/j.soildyn.2013.01.015.

[78] Gasch R, Twele J, Bade P, Conrad W, Heilmann C, Kaiser K, et al. Windkraftanlagen. Wiesbaden: Vieweg+Teubner Verlag; 2005. doi:10.1007/978-3-322-99446-2.

[79] Harte M, Basu B, Nielsen SRK. Dynamic analysis of wind turbines including soil-structure interaction. Eng Struct 2012;45:509–18. doi:10.1016/j.engstruct.2012.06.041.

[80] Bhattacharya S, Adhikari S. Experimental validation of soil-structure interaction of offshore wind turbines. Soil Dyn Earthq Eng 2011;31:805–16. doi:10.1016/j.soildyn.2011.01.004.

[81] Leblanc C, Houlsby GT, Byrne BW. Response of stiff piles in sand to long-term cyclic lateral loading. Géotechnique 2010;60:79–90. doi:10.1680/geot.7.00196.

[82] DNV. Design of Offshore Steel Structures , General - LRFD Method. Det Nor Verit 2011;2018 Ed.:49.

[83] (DNV) Det Norske Veritas. DNV-RP-C203: Fatigue Design of Offshore Steel Structures. 2011.

[84] (DNV) Det Norske Veritas AS. DNV-RP-C101: Design of Offshore steel structures, General (LRFD METHOD. 2011.

[85] (DNV) Det Norske Veritas AS. DNV-OS-J101: Design of Offshore Wind Turbine Structures. 2014.

[86] El-Reedy MA. Marine Structural Design Calculations. Oxford OX5 1GB: Elsevier Ltd; 2015. doi:10.1016/B978-0-08-099987-6.00002-7.

[87] Bhadeshia HKDH. Models for the Elementary Mechanical Properties of Steel Welds. Math Model Weld Phenom III 1997:229–84.

[88] Hansen N. Hall-petch relation and boundary strengthening. Scr Mater 2004;51:801–6. doi:10.1016/j.scriptamat.2004.06.002.

[89] Zhang XF, Han P, Terasaki H, Sato M, Komizo Y. Analytical Investigation of Prior Austenite Grain Size Dependence of Low Temperature Toughness in Steel Weld Metal. J Mater Sci Technol 2012;28:241–8. doi:10.1016/S1005-0302(12)60048-6.

[90] Armstrong RW. 60 Years of Hall-Petch: Past to Present Nano-Scale Connections. Mater Trans 2014;55:2–12. doi:10.2320/matertrans.MA201302.

[91] Dieter G. Mechanical Metallurgy. SI Metric. UK: McGraw-Hill Company; 1988.

[92] Hall EO. The Deformation and Ageing of Mild Steel: III Discussion of Results. Proc Phys Soc Sect B 1951;64:747. doi:10.1088/0370-1301/64/9/303.

[93] Petch NJ. The Ductile-Cleavage Transition in Alpha-Iron. Proc Int Conf Fract 1959:54–67.

[94] Hansen N, Ralph B. The strain and grain size dependence of the flow stress of copper. Acta Metall 1982;30:411–7. doi:10.1016/0001-6160(82)90221-8.

[95] Thompson AW. The comparison of yield and fatigue strength dependence on grain size. Scr Metall 1971;5:859–63. doi:10.1016/0036-9748(71)90059-7.

[96] Phillips WL, Armstrong RW. The influence of specimen size, polycrystal grain size, and yield point behaviour on the fatigue strength of low-carbon steel. J Mech Phys Solids 1969;17:265–70. doi:10.1016/0022-5096(69)90016-7.

[97] Cahn RW, Haasen P. Physical Metallurgy - vol 1. Phys. Metall., vol. 1, 1996, p. 1042.

[98] Becker WT, Lampman S. Fracture appearance and mechanisms of deformation and fracture. Mater Park OH ASM Int 2002 2002;28:559–86. doi:10.1361/asmhba0003537.

[99] Morris, Jr. JW, Guo Z, Krenn CR, Kim Y-H. The Limits of Strength and Toughness in Steel. ISIJ Int 2001;41:599–611. doi:10.2355/isijinternational.41.599.

[100] Yokota T, García Mateo C, Bhadeshia HKDH. Formation of nanostructured steels by phase transformation. Scr Mater 2004;51:767–70. doi:10.1016/j.scriptamat.2004.06.006.

[101] Wronski AS. Comments on - "strengthening mechanisms and brittleness in metals" - by R. W. Armstrong. Ocean Eng 1969;1:257–60. doi:doi:10.1016/0029-8018(69)90026-2.

[102] Callister WDJ. Materials Science and Engineering An Introduction. John Wiley & Sons, Inc; 2007.

[103] Steimbreger C. Fatigue of Welded Structures -Master thesis. Lulea University of Technology, 2014.

[104] Saeed-Akbari A. Determination of steels microstructural components based on novel characterisation techniques. RWTH Aachen, 2008. doi:10.1007/BF03192151.

[105] Thompson SW, Howell PR. Factors influencing ferrite/pearlite banding and origin of large pearlite nodules in a

hypoeutectoid plate steel. Mater Sci Technol 1992;8:777–84. doi:10.1179/mst.1992.8.9.777.

[106]   Chae D, Koss DA, Wilson AL, Howell PR. The effect of microstructural banding on failure initiation of HY-100 steel. Metall Mater Trans A 2000;31:995–1005. doi:10.1007/s11661-000-1017-y.

[107]   Bhadeshia HKDH, Of B, Polish THE, Of A, Sciences T. Phase transformations contributing to the properties of modern steels 2010;58:255–65.

[108]   Korda AA, Mutoh Y, Miyashita Y, Sadasue T, Mannan SL. In situ observation of fatigue crack retardation in banded ferrite-pearlite microstructure due to crack branching. Scr Mater 2006;54:1835–40. doi:10.1016/j.scriptamat.2006.02.025.

[109]   Taylor, J. G., Warin, P. E. and Watson P. Metallographic aspects of fatigue in pearlitic structures. 4th Int. Congr. Fract., vol. 2, Waterloo: Pergamon Press Inc; 1977, p. 681–6.

[110]   Withers PJ, Bhadeshia HKDH. Residual stress. Part 1–measurement techniques. Mater Sci Technol 2001;17:355–65. doi:10.1179/026708301101509980.

[111]   Francis JA, Bhadeshia HKDH, Withers PJ. Welding residual stresses in ferritic power plant steels 2007;23:1009–20. doi:10.1179/174328407X213116.

[112]   Williams S. Welding Distortion and Residual Stresses. Bedford: 2014.

[113]   Cheng X, Fisher JW, Prask HJ, Gnäupel-Herold T, Yen BT, Roy S. Residual stress modification by post-weld treatment and its beneficial effect on fatigue strength of welded structures. Int J Fatigue 2003;25:1259–69. doi:10.1016/j.ijfatigue.2003.08.020.

[114]   Fricke W. Effects of residual stresses on the fatigue behaviour of welded steel structures. Materwiss Werksttech 2005;36:642–9. doi:10.1002/mawe.200500933.

[115]   Hussain, K and De los rios RR. Microstructural effect on tensile and fatigue behaviour of C – Mn steel. J Mater Sci 1997;32:3565–9.

[116]   Rogério dos Santos Alves; Alex Soares de Souza et all. Comparison of Effects of Thermal Aging, Irradiation, and Thermal Annealing on the Propensity for temper Embrittlement on an RPV Submerged-Arc Weld HAZ. Igarss 2014 2014:1–5. doi:10.1007/s13398-014-0173-7.2.

[117]   Kweon KS, Kim JH, Hong JH, Lee CH. Microstructure and toughness of intercritically reheated heat affected zone in reactor pressure vessel steel weld 2000;5:161–7. doi:10.1179/136217100101538155.

[118]   Hamada M. Control of strength and toughness at the heat affected zone. Weld Int 2003;4:265–70. doi:10.1533/wint.2003.3100.

[119]   Hunt a C, Kluken a O, Edwards GR. Heat Input and Dilution Effects in Microalloyed Steel Weld Metals. Weld J 1994;73:S9–15.